ISSN: 2832-1065

Research article

International Journal of Petrochemistry & Natural Gas

Determining The Migration Paths Through Utilization of Pore Pressure, Belayim Land Oil Field, Gulf of Suez, Egypt: a case study

Mahmoud Ghorab[1], Tarek Farag Shazly[1], Ahmed Nooh[1], Mohamed Abu Hassan[2], Mazen. El Bay[2,3], Walid A. Makled[1], Moataz Khaiy Barakat [4,5], Fatma Yehia[1*]

[1] *Exploration Department, Egyptian Petroleum Research Institute (EPRI), Cairo, Egypt.*

[2] *Geology Department, Faculty of Science, Menofia University, Menofia, Egypt.*

[3] *Petro-Services Gmbh Middle East, Cairo, Egypt.*

[4] *Geology Department, Faculty of Science, Tanta University, Tanta, Egypt.*

[5] *Section Organic Geochemistry, GFZ, German Research Centre for Geosciences, Potsdam, Germany.*

[*]Corresponding author
Fatma Yehia. Graduate Researcher, Exploration Department, Egyptian Petroleum Research Institute (EPRI), Cairo, Egypt.

Submitted: 27 Aug 2022; **Accepted:** 01 Sep 2022; **Published:** 27 Sep 2022

Citation: *Mahmoud Ghorab., Tarek Farag Shazly., Ahmed Nooh., Mohamed Abu Hassan., Mazen. El Bay., Walid A. Makled., Moataz Khaiy Barakat ., Fatma Yehia.(2022). Determining The Migration Paths Through Utilization of Pore Pressure, Belayim Land Oil Field, Gulf of Suez, Egypt: a case study. Int J Petro Chem Natur Gas,2(3):85-97.*

Abstract

Deciding on the next wellbore site for field development in oil and gas exploration is a process involving risks and large investments. Selecting a more accurate location based on hydrocarbon migration is one of the ways to reduce the risk in the operations. This study provides an overview to evaluate the pore pressure for main reservoirs in the Belayim oil land fields. These reservoirs are included in the Miocene Belayim, Kareem, and Rudies formations. Calculation of corrected drilling exponent (Dxc) is used in the present research based on electric logs. These calculations specify the pore pressure values and are used to make subsurface mapping that is utilized to observe the migration paths. The study revealed high to low pore pressure in the northeast-southeast trend in Belayim and Kareem formations in the study area. However, the high to low pore pressure trend is inversed and changed to northeast-southwest. Better locations of the field development are located in low pore pressure zones.

Keywords: Eaton's equation; Migration Pathways; Miocene; Gulf of Suez; Belayim Oil Fields; Pore pressure.

Introduction

The Gulf of Suez separates the Sinai Peninsula from the northeast African continent as well as the African and Arabian plates. The Gulf of Suez is considered is one of the most vital hydrocarbon provinces in Africa in general and in Egypt in particular [1]. The earliest exploration phases in the Gulf of Suez started 100 years ago in Ras Gemsa. The exploration was continued thereafter in Belayim Land Field where the study area is located. The study area reaches approximately 113 km2 and hydrocarbons were discovered in 1954. The area of study is confined between longitudes of 33o 12'' (E) and 33o 15'' in the east and latitudes of 28 o 35'' and 28 o 40'' (N) on the eastern coast of the Gulf of Suez (Figure. 1).

This research evaluates the pore pressure of major reservoirs in the study region based on data from 13 wells (112-124, 112-119, 112-100, 112-132, 113-A-54, 113-A-21, 113-155, 113-95, 113-16,113-112, 113-124, 113-124, 113-60, BLSW-1 ST). It aims to construct high-resolution pore pressure distribution maps and to determine migration paths for better development and understanding of hydrocarbon migration direction in the key reservoirs of Belayim, Kareem, and Rudies formations in the Belayim Land Area.

Geological Settings

The Gulf of Suez is distinguished by intervening normal faults that accompanied the rifting in the area since the early Miocene. The network of strike-slip faults that are NE trending produced a compound pattern of grabens and horsts[2] Three provinces are differentiated in the Gulf of Suez based on prevailing structure and dip direction, [3,4]. The research area is situated in the central province and is characterized by the pre-Miocene structural highs and thick Miocene rock succession at shallow depths. These highs were subjected to severe erosion. An anticline trending NS is an essential structural element of the Belayim Land Oil Field. Two main faulting components cut this anticline, the first is parallel to the coast and is represented by some normal faults associated with the Suez graben [5-7]. The other component is represented by a

chain of transcurrent faults subdividing the anticline into several partitions (Figure. 2). Belayim Land Field incorporates a stratigraphic column that extends from Precambrian to Quaternary[8]. The stratigraphic sequence of the central province of the Gulf of Suez is typically represented in the studied succession represented in (Figure. 3), [9-11]. This research focuses on hydrocarbons bearing Belayim, Kareem, and Rudeis formations of the middle and lower parts of Miocene, as shown in (Figure. 4).

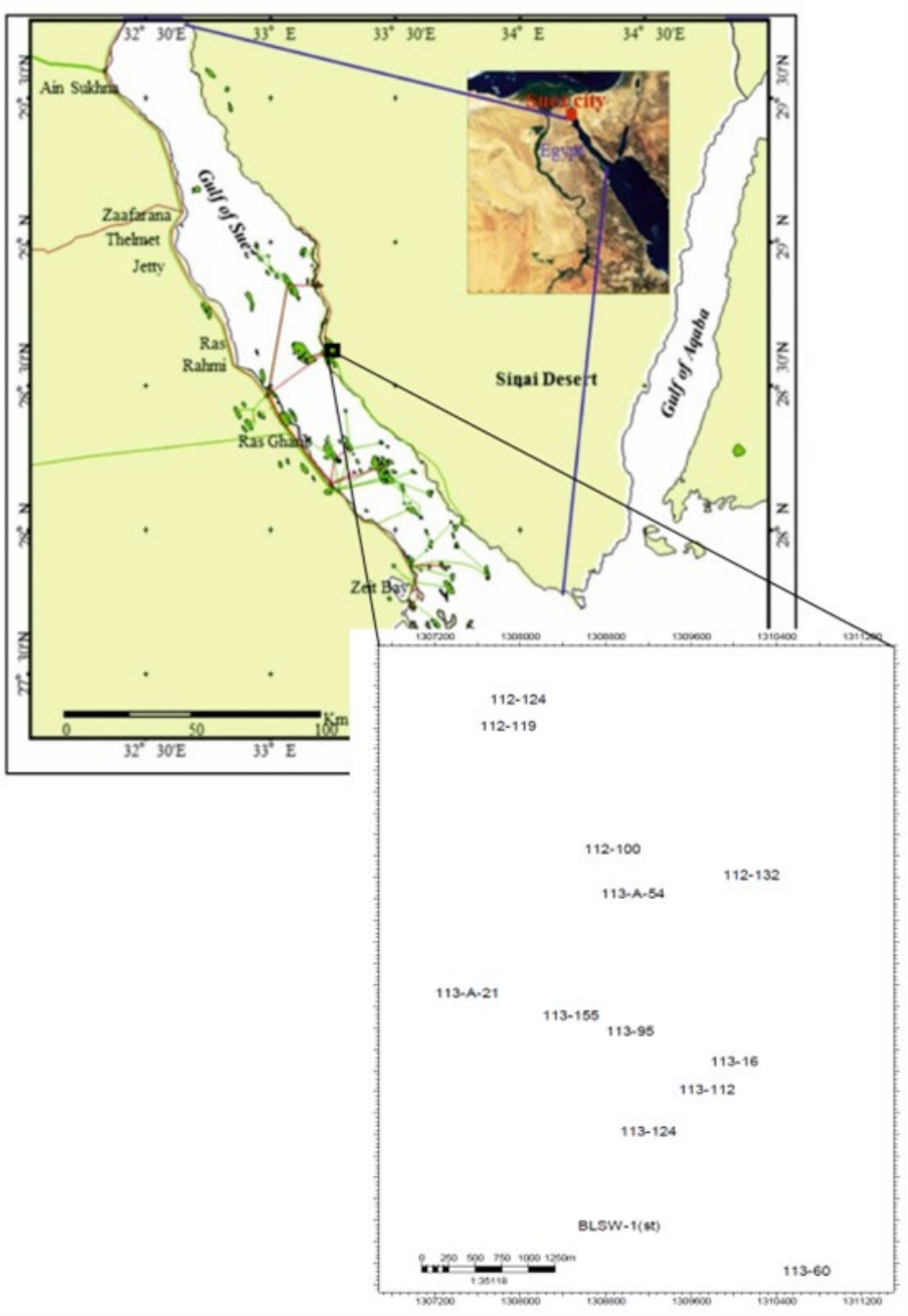

Figure 1: Location map of Belayim Land Field showing the studied wells [12].

Belayim Formation is subdivided into Hammam Farun, Feiran, Sidri, and Baba members and the lithology of these Miocene rock units is as follows:

- Hammam Farun Member: shale and sandstone.
- Feiran Member: anhydrite with intercalations of sandstone and few shale streaks.
- Sidri Member: sandstone and shale.
- Baba Member: anhydrite and salt with shale streaks.
- Kareem Formation: sandstone and shale with intercalations of hard anhydrite.
- Rudeis Formation: sandstone and shale.

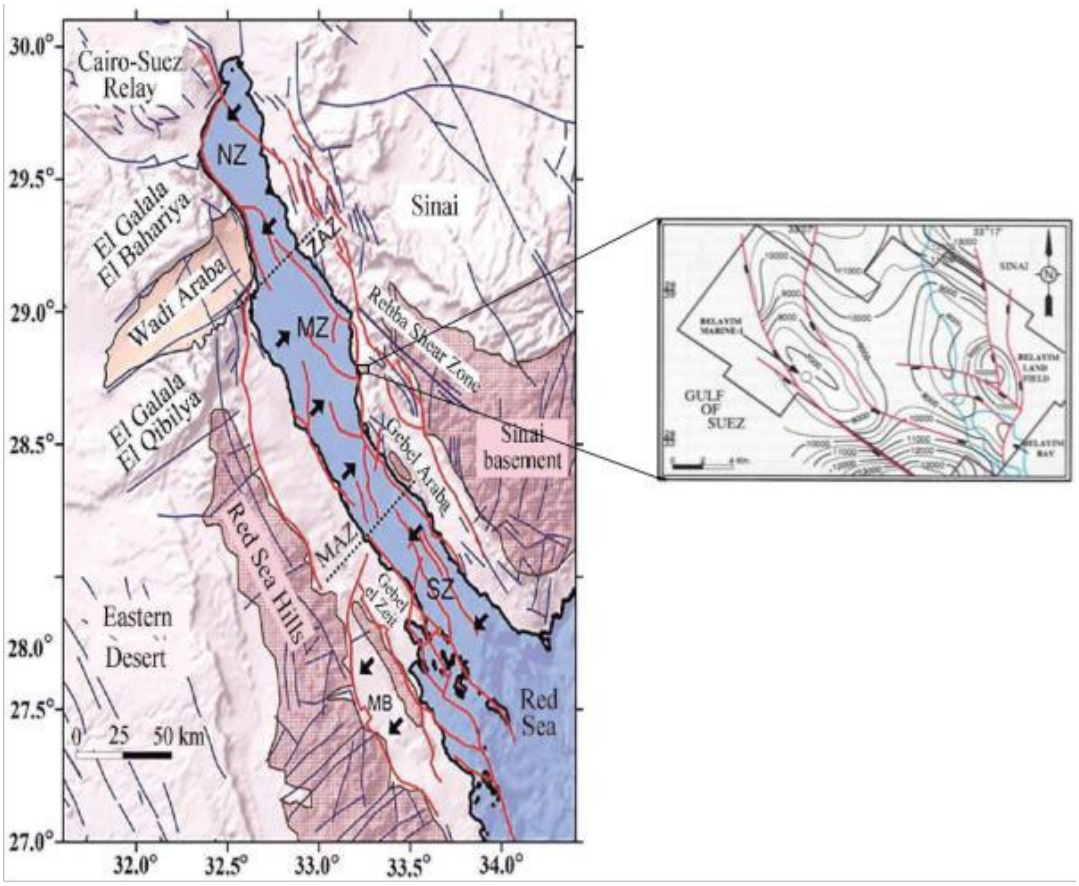

Figure 2: Main structural components in the Gulf of Suez and study area [13].

Materials and Methods

This study is carried out on a dataset from 13 wells as shown in (Figure.1) that are spread in Belayim Land Field (112-124, 112-119, 112-100, 112-132, 113-A-54, 113-A-21, 113-155, 113-95, 113-16,113-112, 113-124, 113-60 and BLSW-1 ST). The well Log analysis process which had been done on electrical logs (Resistivity, Density-Neutron, Sonic, Gamma Ray plus pressure data).

The selected wells were subjected to formation pore pressure evaluation based on corrected drilling exponent Dxc calculation and flow well logging analysis. These data are based mainly on the drilling parameters and well logging data which have been used to make several pressure profiles for the studied wells.

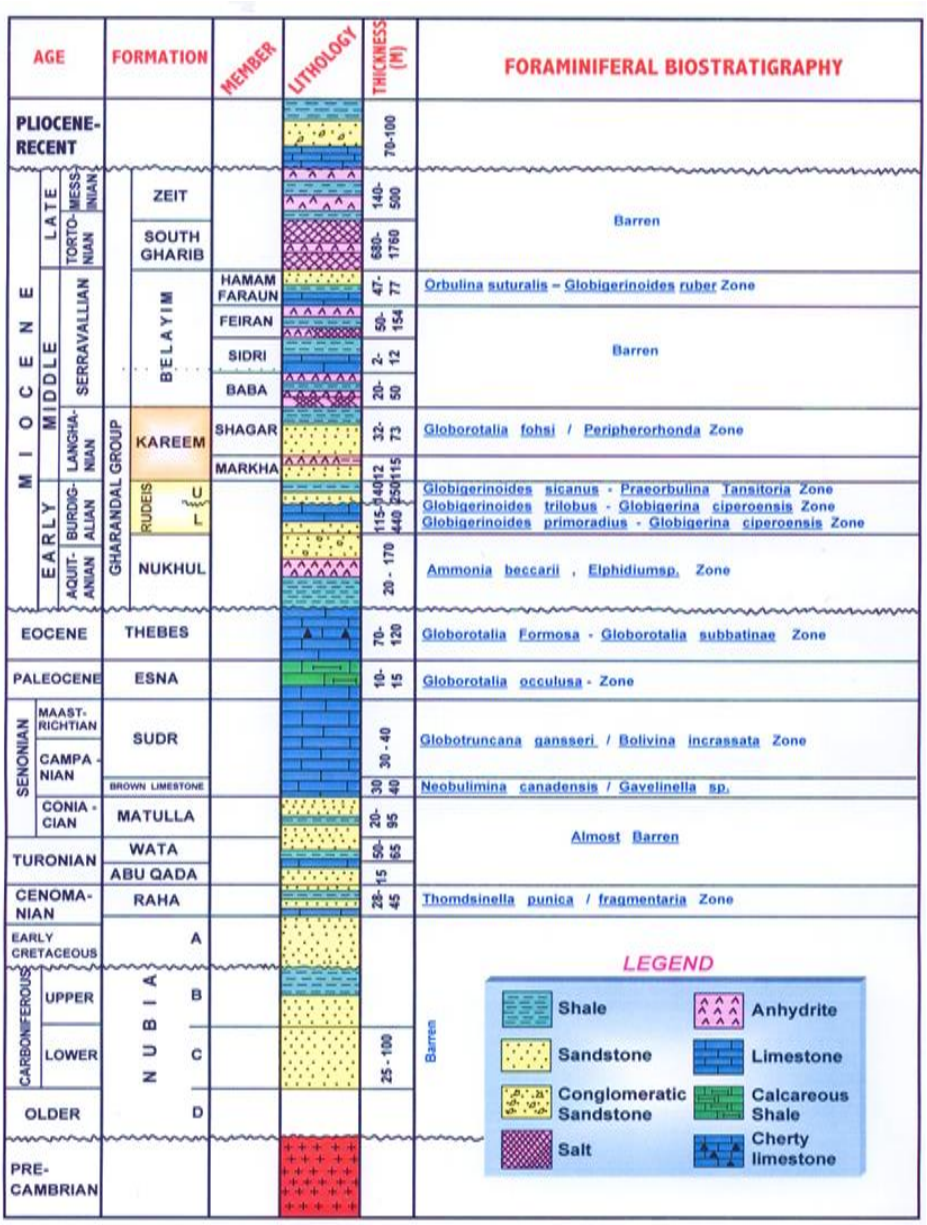

Figure 3: Generalized subsurface stratigraphic section of the Gulf of Suez [14,15].

The pore pressure evaluation is essential for borehole plan and safe drilling and represents an important factor to decrease the risk in drilling operations. Calculations of pore pressure offer geological data that is very useful and valuable for the efficiency of the drilling with the optimum mud weights. This study utilizes the corrected drilling exponent (Dxc) and wireline logs [16].

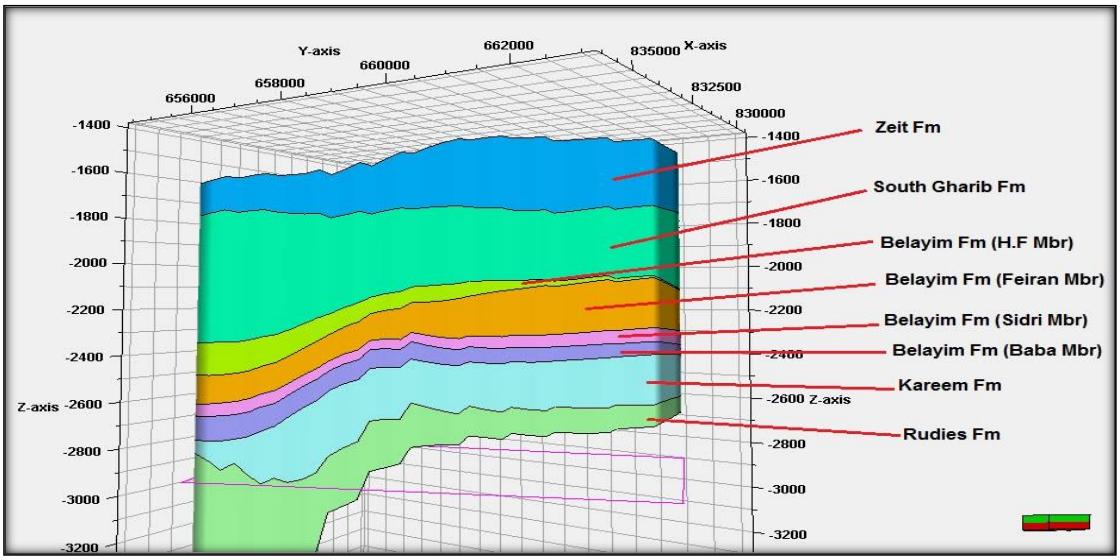

Figure 4: Stratigraphic model for the study area.

Pore Pressure Calculation Based On Drilling Exponents

The exponent is a method that normalizes the penetration rate (ROP) to estimate the hardness or drilling speed throughout rock formation. The method of d-exponent is based on pressure analysis of the formation pores [17,18]. This application is used for normalizing the Bingham drilling model's penetration rate (ROP), concerning the weight on bit parameters (WOB), Rotational velocity (N), and bit diameter (DB). The purpose was to study the link between differential pressure and penetration rate. Differential pressure is the difference between the pressure of the formation pores and the wellbore hydrostatic pressure column [18]. Analysis of such a relationship should make it possible to predict the changes in the pressure of the pores about obtaining. This led to the estimation of a d-exponent beginning with the Bingham drilling model as shown below [17].

The empirical models which are commonly used today include:

a. Model Bingham
b. Jorden and the model Shirley, and
c. Rehm and McClendon, respectively.

Bingham [19]proposed the relationship, which is between the rate of penetration, bit-to-bit weight, rotational speed, and a bit diameter which may be expressed in the first equation. Jorden and Shirley solved the previous equation for “d”, inserted constants to permit common oilfield units to be utilized, and plotted the yield on semi-log paper which delivered values of d-exponent in a helpful workable run [18]. Most imperative, be that as it may, they let “a” be solidarity, expelling must be inferred observational network quality constants, but made the d-exponent lithology particular in the second equation. This correction was suggested by Rehm and McClendon Click or tap here to enter text. according to the third equation [20]. Moreover, Dxc is dimensionless and prone to differential strain, so mud weight can be changed as drilling progresses. In general, if lithology is constant and pore pressure is hydrostatic, Dxc is expected to rise with depth, but decrease in over-pressed zones.

$$B/_N = a\left(W/_B\right)^4 \quad [1]$$

$$D = \log(R/60N)\Big/\log(12W/10^6\,B) \quad [2]$$

$$Dxc = D * N.FBG/ECD \quad [3]$$

A few focuses to be beyond any doubt once you utilize Dxc to identify weight are:

1. Fair utilizing the shale patterns.
2. Patterns will regularly alter with bit and gap estimate changes.
3. Don't utilize in reviewed penetrating or sliding segments.
4. Roller cone bits trend more solid when penetrating.
5. Utilize beside other markers.
6. Deviation from standard pattern indicates transition region, Furthermore, the pore pressure evaluation using d-exponent to thirteen wells in the study area is shown in (Figures.5-12).

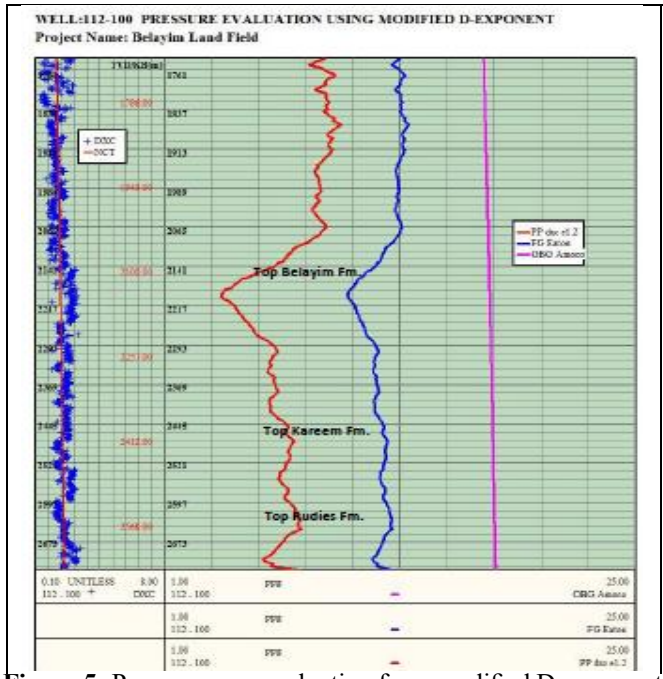

Figure 5: Pore pressure evaluation from modified D-exponent for 112-100 well.

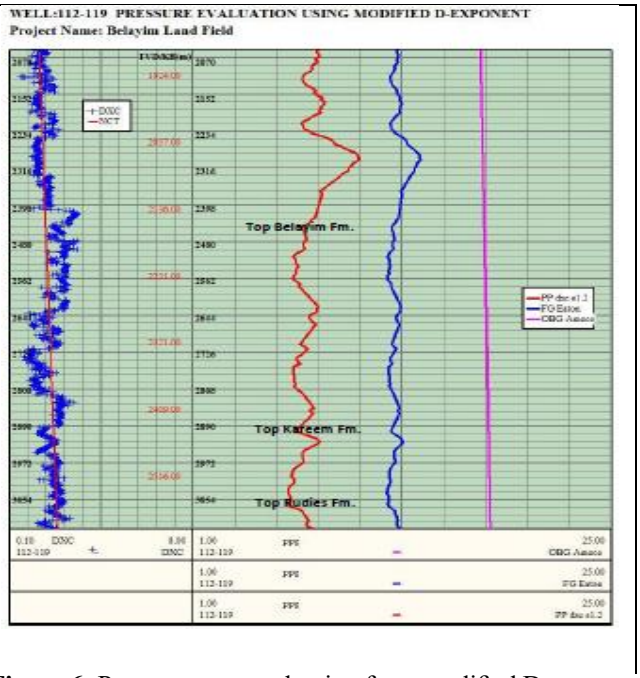

Figure 6: Pore pressure evaluation from modified D-exponent for 112-119 well.

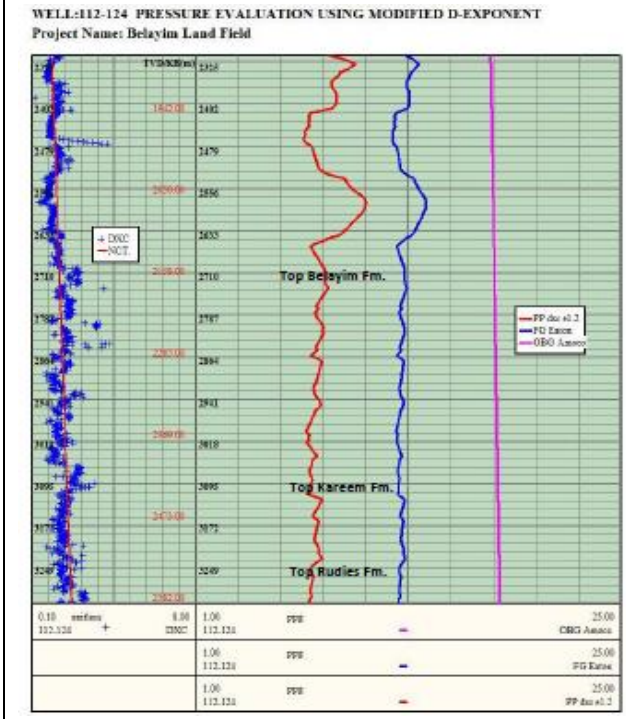

Figure 7: Pore pressure evaluation from modified D-exponent for 112-124 well.

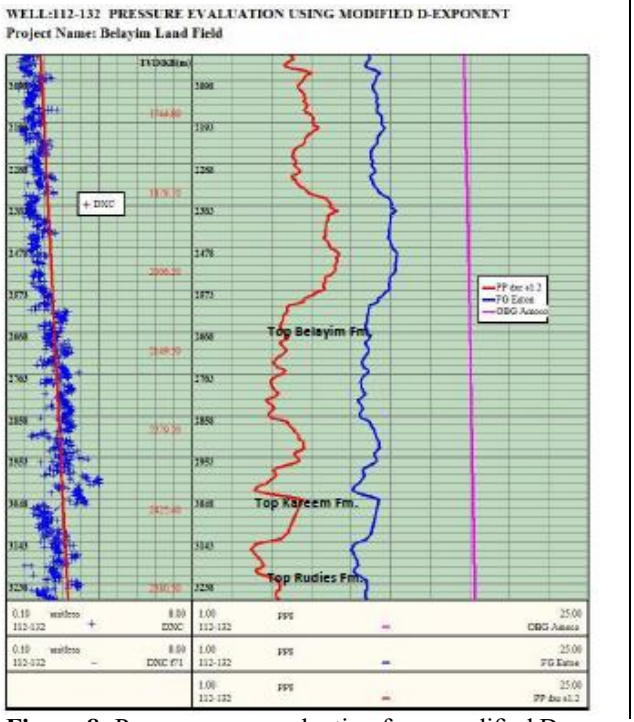

Figure 8: Pore pressure evaluation from modified D-exponent for 112-132 Well.

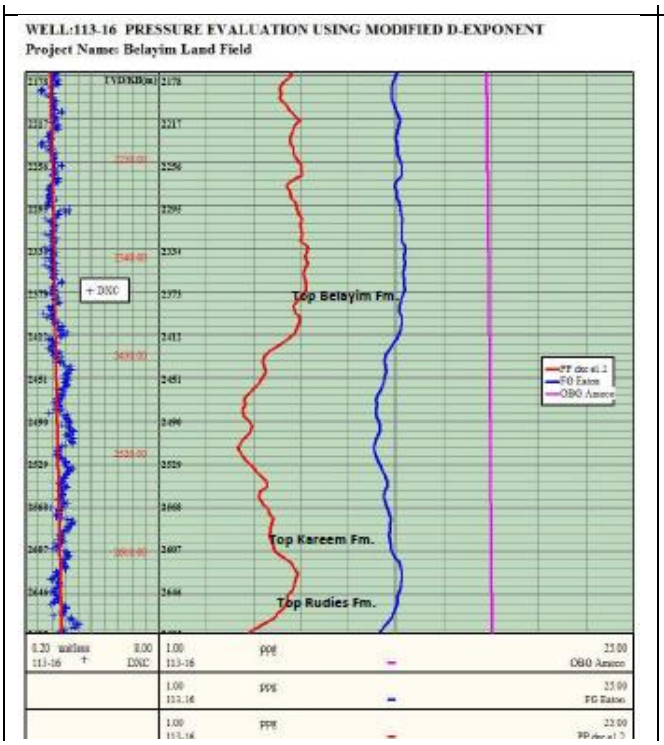

Figure 9: Pore pressure evaluation from modified D-exponent for 113-16 well.

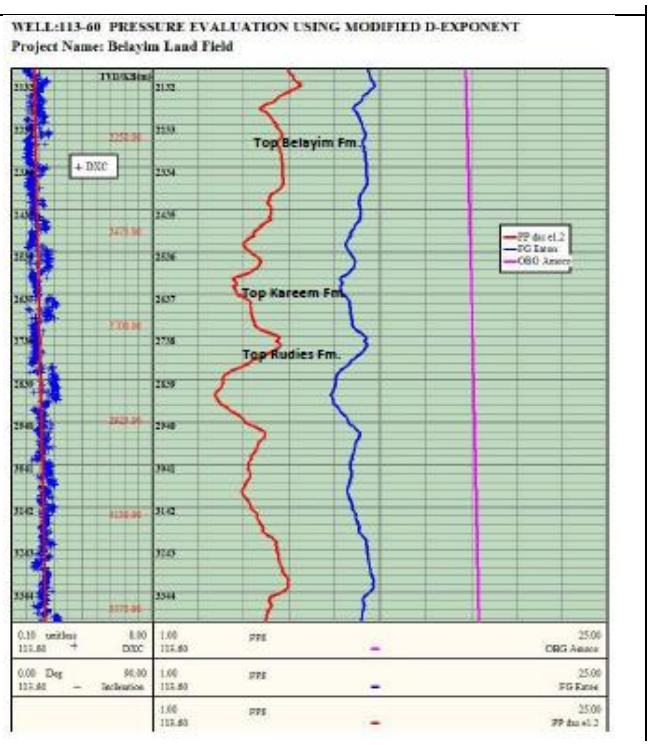

Figure 10: Pore pressure evaluation from modified D-exponent for 113-60 well.

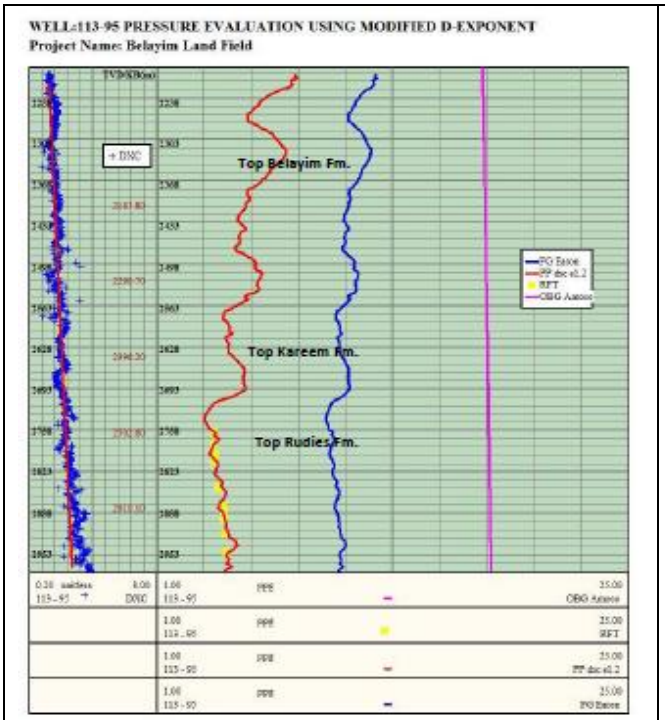

Figure 11: Pore pressure evaluation from modified D-exponent for 113-95 well.

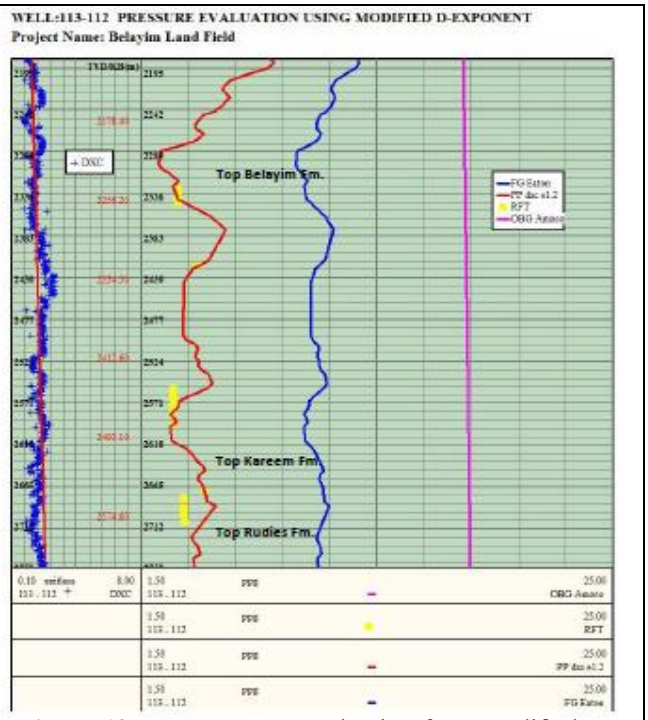

Figure 12: Pore pressure evaluation from modified D-exponent for 113-112 well.

Pore Pressure Estimation Using Wireline Log Parameters

Resistivity Log

One of the most accurate methods of wireline localization is resistivity, which is a measure of an arrangement's ability to conduct an electrical current. Although the pore space may be filled with either non-conductive hydrocarbons or conductive salty water, the strong framework is typically non-conductive. One of the most accurate methods of wireline localization is resistivity, which is a measure of an arrangement's ability to conduct an electrical current. Although the pore space may be filled with either non-conductive hydrocarbons or conductive salty water, the strong framework is typically non-conductive. The values of resistivity are influenced by the sum of permeable liquid with a degree of porosity. Where all perspectives are comparable (homogeneous clay arrangement and steady liquid properties), diminishing within the perused unit of resistivity would result in an increment in a unit of porosity and so overpressure. Hottman and co-workers[21] recommended that a straightforward expression can be a connection between typical and irregular weight in clays according to the following relation between the observed resistivity (R_o) and expected resistivity (R_n) in normally pressured rock at depth under investigation after changing the exponent to 1.5. Additionally, Eaton[22] integrated between the previous equation of pore pressure and the relation of Ro/Rn afterward the equation rewrote as shown in the Fourth equation. Likewise, Eaton[22] employed more advanced analysis and proposed that the value of the exponent be shifted from 1.5 to 1.2 which named as Eaton's equation that mentioned in the fifth equation.

$$R_o/R_n$$

$$P_o = S - (R_o/R_n)^{1.5}\,(S - P_n) \qquad [4]$$

$$P_o = S - (R_o/R_n)^{1.2}\,(S - P_n) \qquad [5]$$

By plotting resistivity logs for clay against profundity and situating the ordinary compaction drift (NCT) on the log, typical resistivity is gotten. Subsequently, Rn is the esteem at the profundity at which pore weight is to be calculated on the NCT. The distinction between Ro and Rn shows at that point the degree of distinction at that profundity between the genuine porosity and typical porosity.

Sonic Log

Sonic travel time (t) can be considered essentially as a lithology and porosity degree. When a given lithology is considered, such as shale, the sonic reaction would essentially be a work of the varieties in porosity. On the off chance that sonic travel times are plotted on a logarithmic scale and a straight scale against profundity, a direct drift will result, and the travel time will diminish profundity. (Eaton, 1975) the condition can be actualized in much the same way as for resistivity on other porosity logs. Mostly, those logs have incorporated with the sonic travel time (Δt) as the following sixth equation.

$$P_o = S - (\Delta\tau_n/\Delta\tau_o)^3\,(S - P_n) \qquad [6]$$

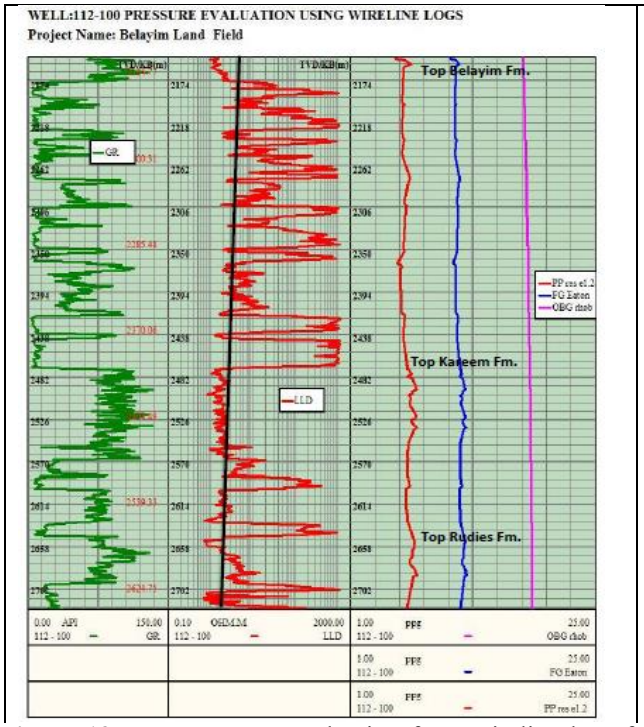

Figure 13: Pore pressure evaluation from wireline logs for 112-100 well.

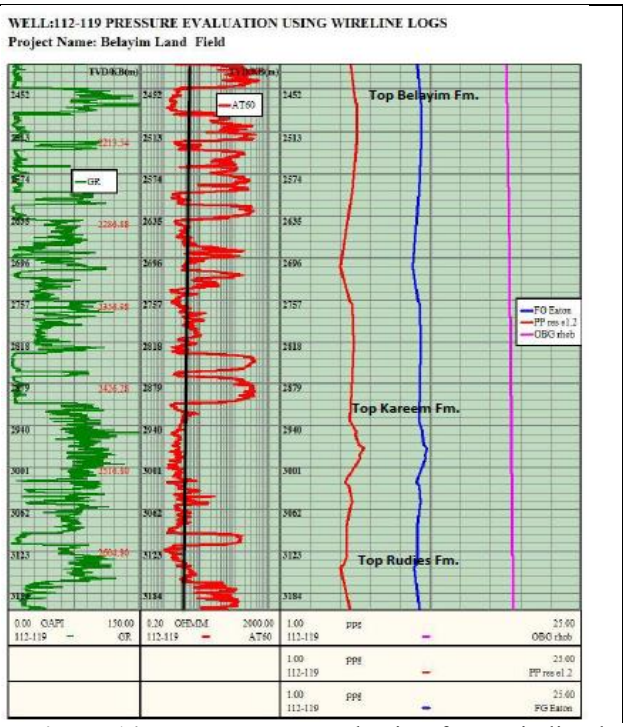

Figure 14: Pore pressure evaluation from wireline logs for 112-119 well.

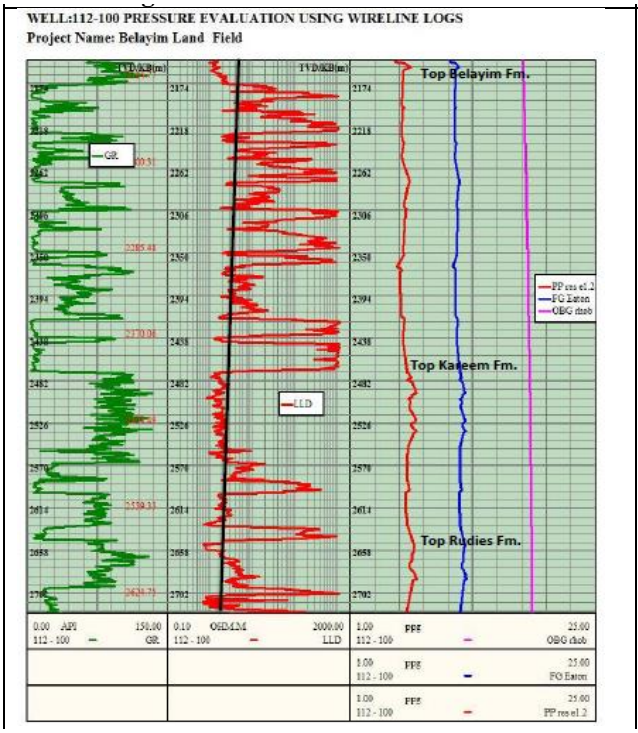

Figure 15: Pore pressure evaluation from wireline logs for 112-100 well.

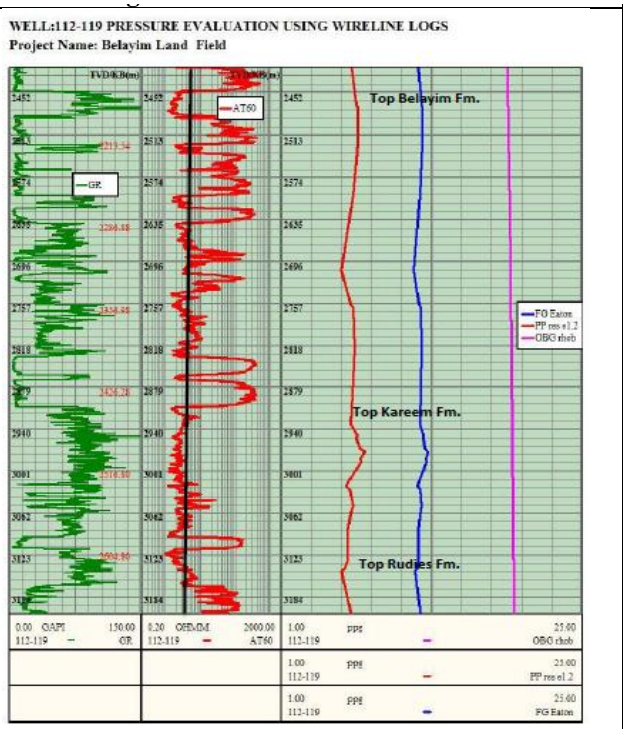

Figure 16: Pore pressure evaluation from wireline logs for 112-119 well.

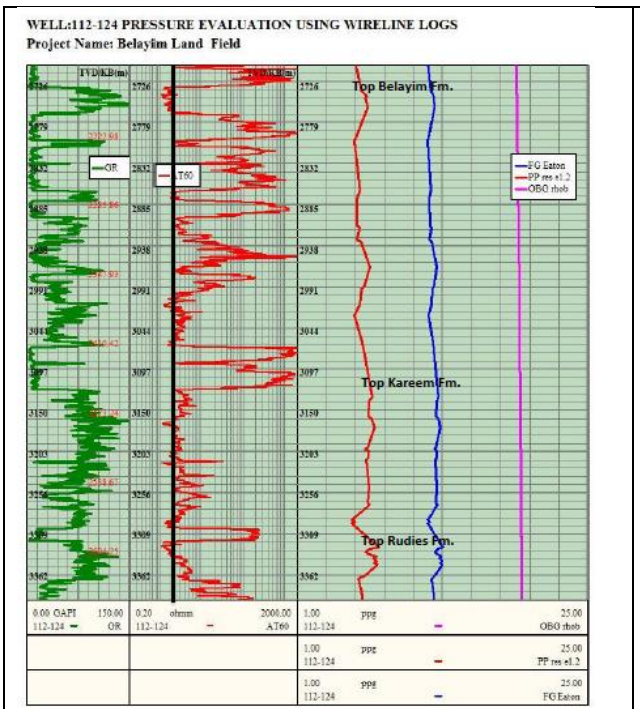

Figure 17: Pore pressure evaluation from wireline logs for 112-124 well.

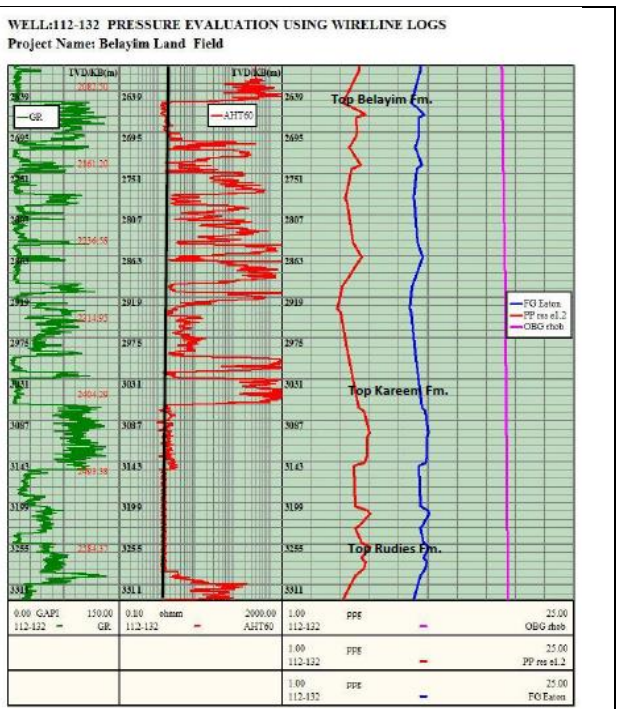

Figure 18: Pore pressure evaluation from wireline logs for 112-132 well.

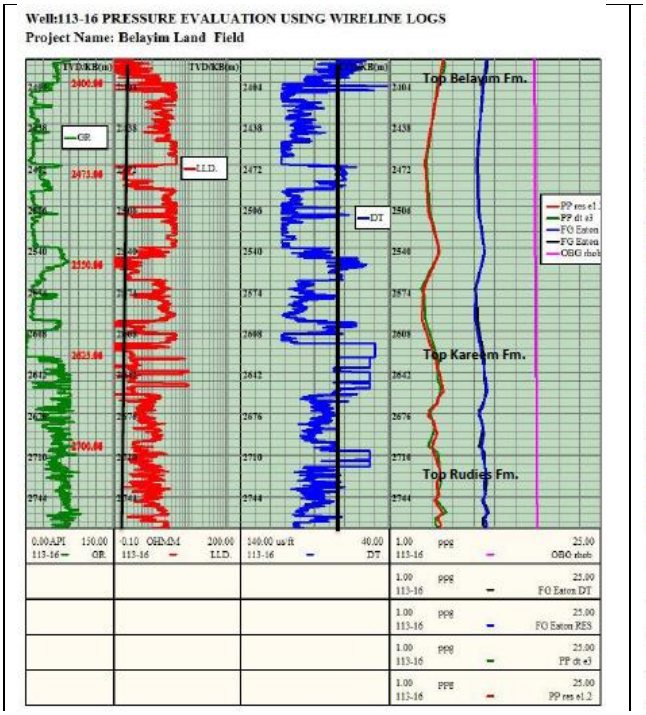

Figure 19: Pore pressure evaluation from wireline logs for 113-16 well.

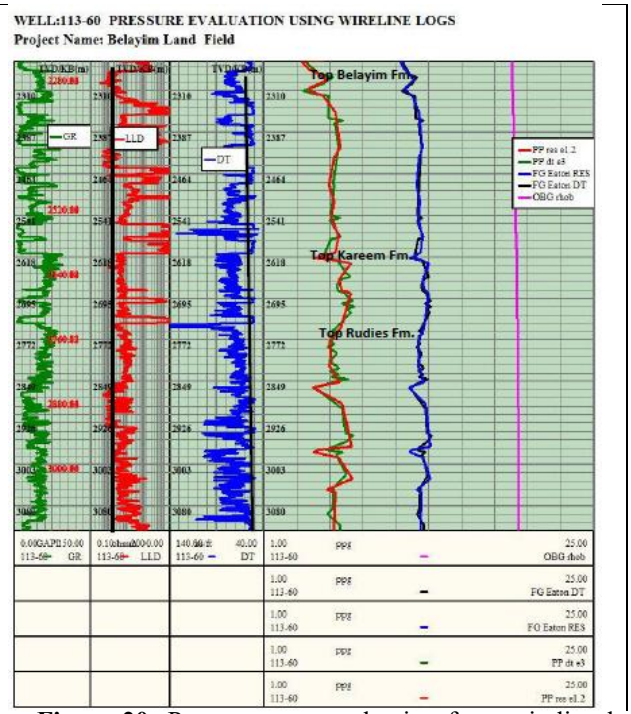

Figure 20: Pore pressure evaluation from wireline logs for 113-60 well.

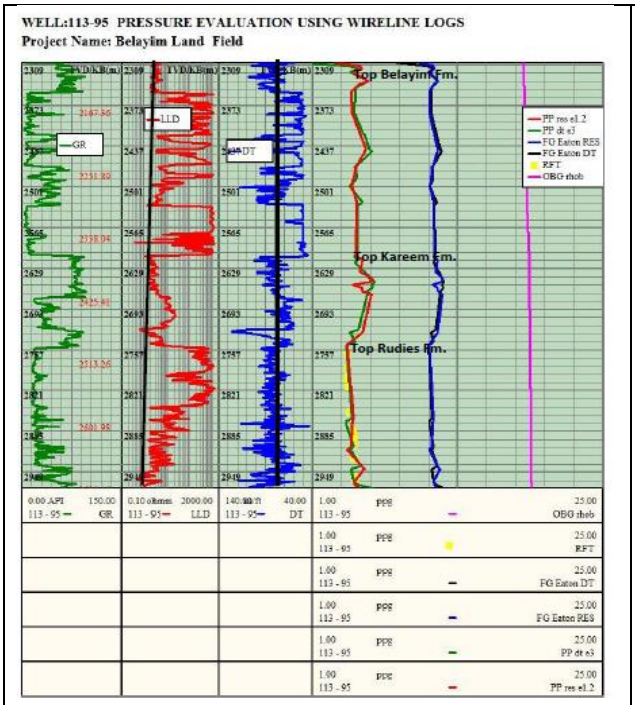

Figure 21: Pore pressure evaluation from wireline logs for 113-95 well.

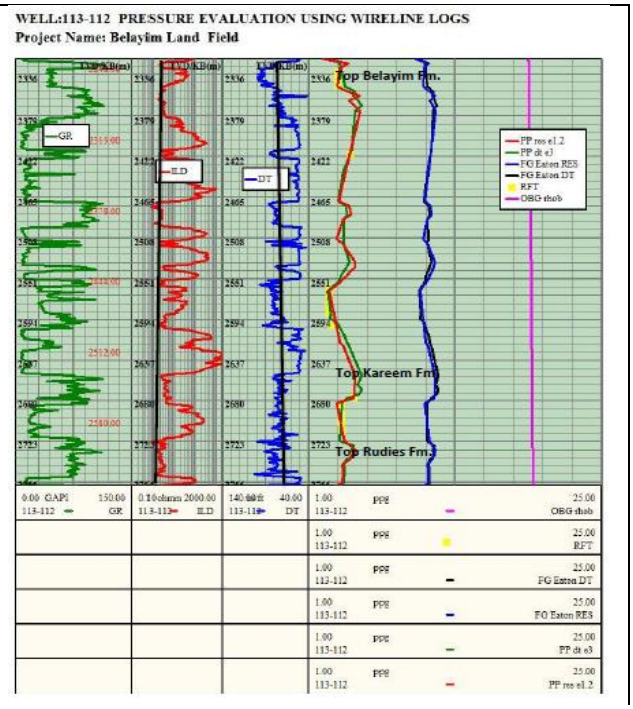

Figure 22: Pore pressure evaluation from wireline logs for 113-112 well.

Results And Discussion

This study is carried out on a dataset from 13 wells that are spread in Belayim Land Field (112-124, 112-119, 112-100, 112-132, 113-A-54, 113-A-21, 113-155, 113-95, 113-16,113-112, 113-124, 113-60 and BLSW-1 ST). The results of pore pressure calculations are used to report any indication of anomaly present in the study area and to study the relationship between pore pressure conditions and the state of faulting variation. This provides the conduits for fluid flow in the migration process from the higher-pressure area to the lower-pressure area and identifies the migration pathways. In the present work, Eaton's equation method was used to evaluate pore pressure and to compare the results with the measured repeat formation tester (RFT) which is represented by yellow points for the reliability of our results. Pore pressure analysis according to [Eaton's] method was applied to the available wells by using the Dxc, resistivity, log, and sonic log trends for main reservoirs. The analysis showed that there is a decrease in pore pressure values as a result of pressure depletion. This depletion is revealed when maximum pore pressure is compared throughout the formation. The lowest pore pressure is found in Belayim Formation (7.9 ppg EMW) then it increases in Kareem Formation (8.25 ppg EMW) and reached a maximum in Rudies Formation (8.3 ppg EMW). This trend indicated an anomalous zone with a deviation of pore pressure.

Pore pressure depletion is recorded and encountered in many areas while drilling for oil and gas. Pressure depletion may occur artificially by extracting hydrocarbon and water from permeable formations which are required and recommended drilling procedures with low mud weight.

In addition, the subsurface maps of pore pressure distribution in the study area showed the location with high and low pore pressure where the lower pore pressure zones represent good locations for development plans.

Pore pressure distribution maps for Belayim Kareem and Rudie's formations are constructed in (Figures. 23-25), and they show that pore pressure is at maximum in the northeast direction and decreases gradually in the southwest direction. The hydrocarbon natural migration paths are from low to high pressure and they will be from northeast to southeast based on the subsurface pore pressure maps basically along the fault plans in the area.

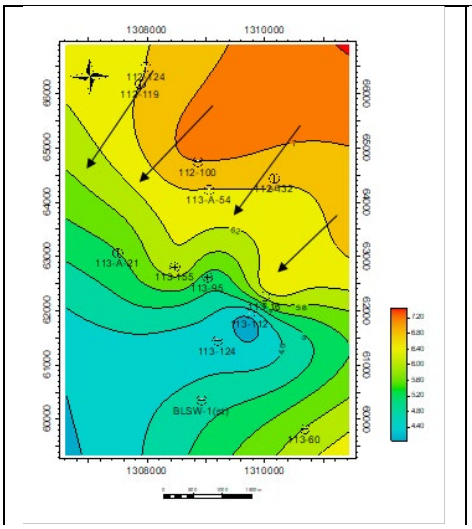

Figure 23: Pore Pressure Distribution Map to Belayim Formation.

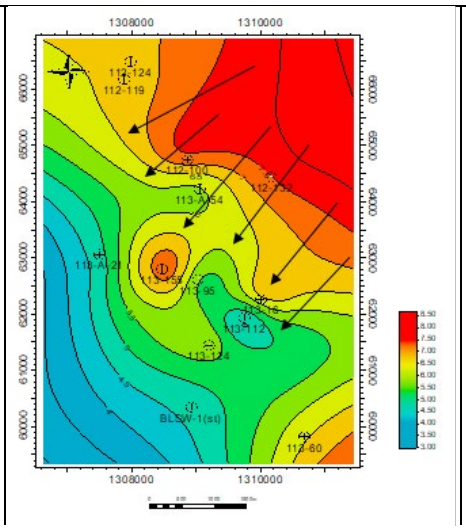

Figure 24: Pore Pressure Distribution Map to Kareem Formation

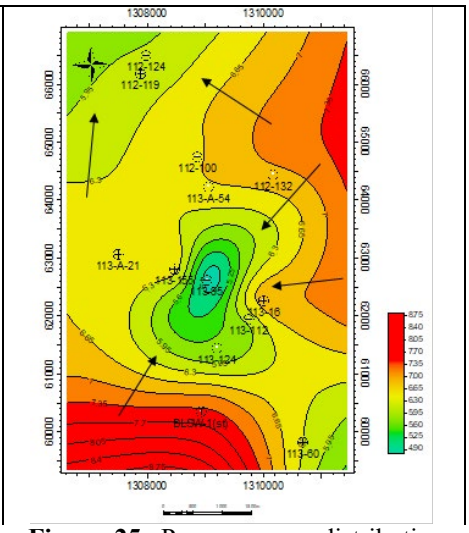

Figure 25: Pore pressure distribution map to Rudies Formation.

Conclusions

This study focused on data of available thirteen wells located in Belayim Land Field. According to the corrected drilling exponent (Dxc) and wireline logs, were utilized for pore pressure evaluation. The lowest pore pressure is found in Belayim Formation (7.9 ppg EMW) where increases in Kareem Formation (8.25 ppg EMW) then reached the maximum in Rudies Formation (8.3 ppg EMW). Moreover, the pore pressure distribution maps of the studied area showed that pore pressure increases in the northeast direction and decreases in the southwest direction in Belayim Kareem and Rudies formations. Accordingly, higher and lower pore pressure zones are determined based on the pressure distribution maps. To conclude that, these zones remark the fluid flow migration paths and additionally the most favourable locations for development plans are the low-pressure zones.

Abbreviations

A	Matrix strength constant (dimensionless).
B	Bit diameter (inches)
D	Drilling exponent (dimensionless)
DXC	D-exponent fixed
ECD	Equivalent circulation density (lb./gal)
N	Rotary speed (rpm)
N. FBG	EQMD (lb./gal) standard forming balance gradient
PN	Normal Pore gradient (Psi/ft)
PO	Pore Pressure Gradient Formation (Psi/ft)
R	Rate of penetration (ft/hr)
S	Overburden Stress Gradient (Psi/ft)
W	Weight on bit (lbs)
ΔT	Transit time (sec/ft)

Reference

1. Barakat, M., & Dominik, W. (2010, June). Seismic Studies on the Messinian Rocks in the Onshore Nile Delta, Egypt. In 72nd EAGE Conference and Exhibition incorporating SPE EUROPEC 2010 (pp. cp-161). European Association of Geoscientists & Engineers.
2. Barakat, M. K., El-Gendy, N., El-Nikhely, A., Zakaria, A., & Hellish, H. (2021). Challenges of the seismic image resolution for gas exploration in the East Mediterranean Sea. Journal of Petroleum and Mining Engineering, 23(2), 13-23.
3. Nabawy, B. S., & Barakat, M. K. (2017). Formation evaluation using conventional and special core analyses: Belayim Formation as a case study, Gulf of Suez, Egypt. Arabian Journal of Geosciences, 10(2), 1-23.
4. El Diasty, W. S., & Peters, K. E. (2014). Genetic classification of oil families in the central and southern sectors of the Gulf of Suez, Egypt. Journal of Petroleum Geology, 37(2), 105-126.
5. Mohamed, H., Saibi, H., Mizunaga, H., & Geith, B. (2022). Basement structure investigation using 3-D forward modeling and inversion of geomagnetic data of the Zeit basin area, Gulf of Suez, Egypt. Marine and Petroleum Geology, 139, 105637.
6. A El-Betar, T., & M Osman, H. (2021). Population structure of Sardinella gibbosa (Bleeker, 1849) with special reference to spawning ground in the Gulf of Suez, Egypt. Egyptian Journal of Aquatic Biology and Fisheries, 25(3), 353-365.
7. Ali, A. M., Radwan, A. E., El-Gawad, A., Esam, A., & Abdel-Latief, A. S. A. (2022). 3D Integrated Structural, Facies and Petrophysical Static Modeling Approach for Complex Sandstone Reservoirs: A Case Study from the Coniacian–Santonian Matulla Formation, July Oilfield, Gulf of Suez, Egypt. Natural Resources Research, 31(1), 385-413.
8. Abuhagaza, A. A., Kassab, M. A., Wanas, H. A., & Teama, M. A. (2021). Reservoir quality and rock type zonation for the Sidri and Feiran members of the Belayim Formation, in Be-

layim Land Oil Field, Gulf of Suez, Egypt. Journal of African Earth Sciences, 181, 104242.
9. Kassab, M., El Gebaly, A., Abass, A., & El Kady, E. (2021). Integrated petrophysical and mineral composition of Miocene reservoirs (Kareem and Belayim Formations), Belayim onshore oil field, Gulf of Suez, Egypt: a case study. Arabian Journal of Geosciences, 14(16), 1-18.
10. Imam, T. S., Abdel-Fattah, M. I., Tsuji, T., & Hamdan, H. A. (2022). Mapping the geological structures in the Ras El Ush field (Gulf of Suez, Egypt), based on seismic interpretation and 3D modeling techniques. Journal of African Earth Sciences, 104596.
11. Elmaadawy, K. (2021). Oil characteristics and source rock potential of Abu Rudeis-Abu Zenima area, Central province, Gulf of Suez, Egypt. Journal of Petroleum and Mining Engineering, 23(2), 1-12.
12. Alsharhan, A. S. (2003). Petroleum geology and potential hydrocarbon plays in the Gulf of Suez rift basin, Egypt. AAPG bulletin, 87(1), 143-180.
13. Sarhan, M., & Hemdan, K. (1994). North Nile Delta structural setting and trapping mechanism, Egypt. In Proceedings of the 12th Petroleum Conference of EGPC (Vol. 12, No. 1, pp. 1-17).
14. Radwan, A. E., Rohais, S., & Chiarella, D. (2021). Combined stratigraphic-structural play characterization in hydrocarbon exploration: a case study of Middle Miocene sandstones, Gulf of Suez basin, Egypt. Journal of Asian Earth Sciences, 218, 104686.
15. Mahmoud, K. O. R. A. (1998). The Permo-Carboniferous outcrops of the Gulf of Suez region, Egypt: stratigraphic classification and correlation. Geodiversitas, 20(4).
16. G. L. Bowers, "Pore pressure estimation from velocity data: Accounting for overpressure mechanisms besides undercompaction," SPE Drilling & Completion, vol. 10, no. 02, pp. 89–95, 1995.
17. Bourgoyne, A. T., Millheim, K. K., Chenevert, M. E., & Young, F. S. (1991). Applied drilling engineering, revised 2nd printing. Society of Petroleum Engineering, Richardson, TX, 246-667.
18. Jorden, J. R., & Shirley, O. J. (1966). Application of drilling performance data to overpressure detection. Journal of Petroleum Technology, 18(11), 1387-1394.
19. Bingham, G. (1965). A new approach to interpreting rock drillability. TECHNICAL MANUAL REPRINT, OIL AND GAS JOURNAL, 1965. 93 P.
20. Rehm, B., & McClendon, R. (1971, October). Measurement of formation pressure from drilling data. In Fall Meeting of the Society of Petroleum Engineers of AIME. OnePetro.
21. Hottmann, C. E., & Johnson, R. K. (1965). Estimation of formation pressures from log-derived shale properties. Journal of Petroleum Technology, 17(06), 717-722.
22. Eaton, B. A. (1975, September). The equation for geopressure prediction from well logs. In Fall meeting of the Society of Petroleum Engineers of AIME. OnePetro.